The 5th Joint International Conference on Multibody System Dynamics
June 24 –28, 2018, Lisbon, Portugal

Solution of the general single contact frictional problem in multibody dynamics using b-geometry

Sotirios Natsiavas[1] and Elias Paraskevopoulos[2]

[1] *Department of Mechanical Engineering, Aristotle University, Thessaloniki, Greece, natsiava@auth.gr*
[2] *Department of Mechanical Engineering, Aristotle University, Thessaloniki, Greece, eapcivil@gmail.com*

ABSTRACT — *This study presents a new formulation of the dynamics of systems involving a single frictional contact. An analytical dynamics framework is employed, together with some fundamental tools of differential geometry. This provides a foundation for applying Newton's law of motion to systems possessing configuration manifolds with boundary. Based on this, it is shown that the contact phase takes place inside a thin boundary layer, where the dominant dynamics is described by a set of three ordinary differential equations. The study includes a selected set of examples, with emphasis put on investigating phenomena arising during central or eccentric collision of solid bodies.*

1 Introduction

Dynamics of systems possessing mechanical components that come in contact during their motion is a classical subject of Mechanics (e.g., [1-6]). This is due to both its large practical significance and the challenging theoretical issues arising in the effort to predict and understand the various phenomena observed and related to contact events. Previous studies have demonstrated that friction effects are responsible for the appearance of a plethora of new phenomena during impact. Based on the type of approach adopted, these studies can roughly be divided in two general categories. In the first category, the contact event is assumed to take place in an instantaneous manner. This leads to the appearance of a discontinuity in the velocities, accompanied by unbounded contact forces in order to avoid interpenetration. This, in turn, leads to the necessity of employing techniques of the so-called Nonsmooth Mechanics (e.g., [1-5]). In essence, these approaches lead to prediction of the post-impact velocities through an algebraic process, making use of the pre-impact velocities and appropriate restitution coefficients. On the other hand, the second category of previous studies on systems with unilateral constraints is based on the Darboux-Keller approach (e.g., [6-10]). Their common characteristic is that they consider the normal impulse as an independent time-like variable and lead to a set of equations of motion during the contact phase in the form of ordinary differential equations (ODEs).

The present study is a continuation of earlier work of the authors [11,12] and applies to a class of constrained mechanical systems, involving a single impact event with friction. The approach taken is novel compared to previous studies on the subject. In particular, the analysis applied is carried out within the classical framework of analytical dynamics and can handle systems with general properties, including rigid and discretized deformable bodies. The formulation is based on a proper application of Newton's law of motion during the contact phase. The final outcome is a completely continuous formulation, in contrast to the approaches based on non-smooth techniques. This is achieved through the use of some key ideas and concepts of b-geometry, which provide a natural and strong setting for studying mechanical systems subject to a unilateral constraint [13]. Namely, after defining the boundary of the configuration manifold and determining the essential geometric properties needed for the application of the law of motion inside a thin layer starting at this boundary, it is shown that the dominant dynamics during a single frictional collision is described by a set of three coupled ODEs. These equations describe action in a three dimensional distribution of the configuration manifold, which is related directly to the action in

the physical space, where the contact event examined takes place. Using time as an independent variable presents an advantage over the Darboux-Keller approaches, since it provides a valuable time scale for investigating the part of the motion inside the boundary layer. Moreover, the general spirit of the new approach is entirely different. Instead of modeling the contact with stiff springs, which demands to give up the rigidity assumption in case of a rigid body contact, application of the theory for a manifold with boundary reveals that the associated contact action is modeled by a large change in the inertia properties [13], in combination with the appearance of a strong repulsive force. More specifically, the components of the metric and the connection employed along the normal to its boundary vary in a quite rapid fashion in the vicinity of the boundary in the configuration space. This causes a fast deceleration of the figurative particle modeling the motion of the mechanical system in the configuration manifold, as it approaches the boundary. Also, once this particle enters the boundary layer, it is pushed away from it by a strong repulsive force, which is exerted on it until its exit from the boundary [12].

In the second part of this study, the attention is shifted on applying the new analysis to investigating collision of a particle with a rigid wall and continues with examination of central and eccentric collisions of solid bodies. The more accurate modeling provides a strong basis and leads to a better understanding of the phenomena involved. Finally, the analysis is presented in a way that permits its extension to more complex problems, involving situations with multiple contacts [14].

The organization of this paper is as follows. First, the general theoretical setting is presented in the following section. Then, the essential geometric properties are presented in Section 3. This information is employed in Section 4, where the equations governing the motion during the contact phase are derived. Next, a critical comparison with previous formulations is presented in Section 5, while several characteristic examples are examined in Section 6. Finally, the new findings are briefly summarized in the last section.

2 Manifolds with boundary and mechanical systems with contact

This study is a continuation of recent work of the authors on the dynamics of mechanical systems subject to unilateral constraints [12]. The new ingredient is that the contact involves frictional effects. Adopting the general framework of Analytical Dynamics, the spatial configuration of the system is described by a finite set of generalized coordinates, $q=(q^1,\ldots,q^n)$, selected to be minimal. These are related to a fictitious point p, moving as a function of time t on an n-dimensional manifold M, the configuration manifold of the unconstrained system [15]. Then, the presence of a contact event is signaled by an inequality condition

$$\rho(p)\geq 0\,, \tag{1}$$

assuring no interpenetration. The equality in this condition defines a hypersurface in M and the motion of point p occurs on one side of this hypersurface only. In this way, the function ρ acts as a boundary defining function on manifold M and gives rise to a new manifold

$$X=\{p\in M:\ \rho(p)\geq 0\}\,,$$

with dimension n [13]. This manifold possesses a boundary ∂X and an interior $X^o=X\setminus\partial X$. Then, the new manifold is represented by the disjoint union

$$X=X^o\coprod\partial X\,,$$

while the motion of the class of systems examined is represented by a curve on the constrained manifold X. The tangent vector to such a curve at a point p belongs to an n-dimensional vector space T_pX, the tangent space at p. Therefore, if $\mathfrak{B}_e=\{\underline{e}_1\ \ \ldots\ \ \underline{e}_n\}$ is a basis of T_pX, then any of its elements can be put in the form

$$\underline{u}=u^I\underline{e}_I=u^1\underline{e}_1+u^i\underline{e}_i\,,$$

with the summation conventions

$$u^I \underline{e}_I = \sum\nolimits_{I=1}^{n} u^I \underline{e}_I \quad \textit{and} \quad u^i \underline{e}_i = \sum\nolimits_{i=2}^{n} u^i \underline{e}_i \,,$$

so that a capital Latin index ranges from 1 to n and a lower case Latin index runs from 2 to n.

The tangent space at each point of X is accompanied by a cotangent space, denoted by $T_p^* X$. In fact, to each vector $\underline{u}$ of $T_p X$ there corresponds a covector $\underset{\sim}{u}^*$ of $T_p^* X$. In dynamics, it is convenient to establish this correspondence by using the following dual product

$$\underset{\sim}{u}^*(\underline{w}) = \langle \underline{u}, \underline{w} \rangle \,, \quad \forall \underline{w} \in T_p X \tag{2}$$

where $\langle \cdot, \cdot \rangle$ represents the inner product of the vector space $T_p X$. In this way, for any basis $\mathfrak{B}_e$ of $T_p X$, a dual basis $\mathfrak{B}_e^* = \{\underset{\sim}{e}^1 \quad \dots \quad \underset{\sim}{e}^n\}$ can be obtained for $T_p^* X$, by employing the conditions $\underset{\sim}{e}^I(\underline{e}_J) = \delta_J^I$, where $I, J = 1, \dots, n$ and the symbol in the right hand side denotes a Kronecker's delta [15]. Finally, definition of the vector spaces $T_p X$ and $T_p^* X$ at each point of manifold X is essential in creating two other spaces, by

$$TX = \coprod_{p \in X} T_p X \quad \textit{and} \quad T^* X = \coprod_{p \in X} T_p^* X \,,$$

known as the tangent and cotangent vector bundles over X, respectively [16].

If $V(X)$ denotes the space of all smooth vector fields on X, the integration of its elements to obtain the corresponding flows is not closed on X. To fix this problem, the theory of manifolds with boundary, or b-manifolds [13], is employed. In particular, these vector fields are elements of the space

$$V_b(X) \equiv \{V \in V(X) : \, V \text{ is tangent to } \partial X\} \,.$$

This means that if the local coordinates $x = (x^1, \dots, x^n)$ are introduced at a point p of the boundary ∂X, so that $\rho = x^1 \geq 0$, then any element of a vector field belonging to $V_b(X)$ can be put in the form

$${}^b\underline{v} = \alpha x^1 \underline{g}_1 + a^i \underline{g}_i \,, \tag{3}$$

over a holonomic basis $\mathfrak{B}_g = \{\underline{g}_1, \underline{g}_2, \dots, \underline{g}_n\}$, where $\underline{g}_I \equiv \partial / \partial x^I$ are tangent vectors to the coordinate lines starting at p [15]. Therefore, the special set ${}^b\mathfrak{B}_g = \{x^1 \underline{g}_1, \underline{g}_2, \dots, \underline{g}_n\}$ forms a basis for $V_b(X)$ at each point near the boundary. The first element of this set vanishes at points on the boundary, but it can be shown that there exists a new vector bundle over X, denoted by ${}^bTX$, where the component vector space ${}^bT_p X$ is n-dimensional even at points of the boundary ∂X [13]. A companion b-cotangent bundle ${}^bT^* X$ can also be defined in a similar manner. Then, at a point p of ∂X, a typical element of ${}^bT^* X$ can be expressed in the form

$${}^b\underset{\sim}{v}^* = \beta \frac{dx^1}{x^1} + b_i dx^i \,, \tag{4}$$

with $dx^I \equiv \underset{\sim}{g}^I$. This demonstrates that the set ${}^b\mathfrak{B}_g^* = \{dx^1 / x^1, dx^2, \dots, dx^n\}$ represents a basis of ${}^bT_p^* X$ near the boundary. Finally, both the b-tangent bundle ${}^bTX$ and the b-cotangent bundle ${}^bT^* X$ coincide with the ordinary bundles TX and $T^* X$, respectively, away from the boundary (for more details, see [13] and [12]).

3 Essential geometric properties of a manifold with boundary

In determining the geometric properties of manifold X, it is convenient to employ two special bases in ${}^bT_p X$. The first corresponds to a local x-coordinate system, as defined at the end of the previous section, while the second is related to the original q-coordinate system, denoted by $\mathfrak{B}_e = \{\underline{e}_1 \quad \dots \quad \underline{e}_n\}$ and $\mathfrak{B}_{e'} = \{\underline{e}_1 \quad \dots \quad \underline{e}_{n'}\}$, respectively. Then, any element of ${}^bT_p X$ can be expressed in the following two alternative forms

$${}^b\underline{v} = \dot{x}^I \underline{e}_I = \dot{q}^{I'} \underline{e}_{I'} \,.$$

By considering the corresponding transformation between $\mathfrak{B}_e$ and $\mathfrak{B}_{e'}$, expressed in the form

$$\underline{e}_{I'} = A_{I'}^I \underline{e}_I \quad \textit{or} \quad \underline{e}_I = B_I^{I'} \underline{e}_{I'} \,, \tag{5}$$

for $I, I' = 1,\ldots,n$ [15], the components of a b-vector in those bases are related by

$$\dot{x}^I = A^I_{I'}\,\dot{q}^{I'} \quad and \quad \dot{q}^{I'} = B^{I'}_I\,\dot{x}^I\,, \tag{6}$$

where matrix $A = [A^I_{I'}]$ is the inverse of matrix $B = [B^{I'}_I]$.

Within this setting, the components of the b-metric tensor can now be obtained. This tensor has components $\overline{g}_{IJ} = \overline{g}_{JI} = \langle \underline{e}_I, \underline{e}_J \rangle$ with respect to a basis of the x-coordinate system and is virtually unaffected by the presence of the boundary at points away from the boundary ∂X, i.e.,

$$\overline{g}_{IJ} = g_{IJ} \quad over\ X^o\,, \tag{7}$$

with $G = [g_{IJ}]$. Near the boundary, the b-metric is affected in a significant way [13]. In particular, one can always find a special x-coordinate system, where the metric matrix can be put in the block diagonal form

$$\overline{G} = [\overline{g}_{IJ}] = \begin{bmatrix} \overline{g}_{11} & \underline{0}^T \\ \underline{0} & \overline{G}_T \end{bmatrix}, \tag{8}$$

with

$$\overline{g}_{IJ} = g_{IJ} + \hat{g}_{IJ}\,. \tag{9}$$

The term $\hat{g}_{IJ}$ is solely due to the presence of the boundary and appears in the explicit form

$$\hat{g}_{11} = \widehat{g}_{11} \big/ (x^1)^2 \quad and \quad \hat{g}_{i1} = \hat{g}_{1j} = \hat{g}_{ij} = 0\,. \tag{10}$$

By employing the basis transformation expressed by Eq. (5), the metric components in the x-coordinate system can be related to the components of the metric with respect to the q-coordinate system [15], through

$$g_{IJ} = B^{I'}_I B^{J'}_J g_{I'J'} \quad and \quad g_{I'J'} = A^I_{I'} A^J_{J'} g_{IJ}\,. \tag{11}$$

Then, using Eq. (9), it is easily obtained that near the boundary

$$\overline{g}_{I'J'} = g_{I'J'} + \hat{g}_{I'J'}\,, \tag{12}$$

which is similar in form to Eq. (9). Moreover, taking into account Eq. (11), the last term is obtained through

$$\hat{g}_{I'J'} = A^1_{I'} A^1_{J'} \hat{g}_{11}\,.$$

Clearly, only the first line of matrix $A = [A^I_{I'}]$ needs to be specified for determining $\hat{g}_{I'J'}$, which is evaluated by

$$A^1_{I'} = \underset{\sim}{e}^1(\underline{e}_{I'}) = \langle \nabla\rho, \underline{e}_{I'} \rangle\,, \tag{13}$$

so that the gradient vector $\nabla\rho$ is normal to the boundary hypersurface defined by $\rho(q) = 0$.

Next, in analogy to Eq. (9), the b-affinities are also decomposed in the form

$$\overline{\Lambda}^K_{IJ} = \Lambda^K_{IJ} + \mathrm{A}^K_{IJ}\,, \tag{14}$$

with respect to a basis of the x-coordinate system. The terms Λ^K_{IJ} coincide with the affinities of the ordinary vector bundle TX, defined over the extension manifold M, while A^K_{IJ} are terms arising from the presence of the boundary. The latter terms are negligible away from ∂X, so that

$$\overline{\Lambda}^K_{IJ} = \Lambda^K_{IJ} \quad over\ X^o\,. \tag{15}$$

Moreover, the correction terms A^K_{IJ} in Eq. (14) are in fact components of a tensor [12]. Also,

$$\overline{\Lambda}^{K'}_{I'J'} = \Lambda^{K'}_{I'J'} + \mathrm{A}^{K'}_{I'J'}\,, \tag{16}$$

which has a similar structure to Eq. (14), while the component A^1_{11} has the following form

$$\mathrm{A}^1_{11} \approx \bar{\Lambda}^1_{11} = -1/x^1 . \tag{17}$$

This term contributes to all the b-affinities of the q -coordinate system through

$$\mathrm{A}^{K'}_{I'J'} = A^1_{I'} A^1_{J'} B^{K'}_1 \mathrm{A}^1_{11} ,$$

which involves only terms of the form $A^1_{I'}$ and $B^{I'}_1$ [12]. The first of them are determined by Eq. (13). In addition, using Eqs (5) and (11) together with the identity $g^{I'J'} g_{J'K'} = \delta^{I'}_{K'}$, it can be shown that

$$B^{I'}_I = g^{I'J'} A^J_{J'} g_{JI} .$$

Therefore,

$$B^{I'}_1 = g^{I'J'} A^1_{J'} g_{11} ,$$

which implies that $B^{I'}_1$ can be evaluated by knowledge of the known components $A^1_{I'}$ only. Moreover, the affinities Λ^K_{IJ} are transformed back to the basis of the q -coordinate system by

$$\Lambda^{K'}_{I'J'} = A^I_{I'} A^J_{J'} B^{K'}_K \Lambda^K_{IJ} + B^{K'}_K A^K_{J',I'} .$$

4 Equations of motion for the problem of single contact with friction

The true path of the figurative particle representing the motion on the configuration manifold is determined by application of Newton's law [11,16]. On a manifold without boundary, this law is expressed in the form

$$\nabla_{\underline{v}} \underset{\sim}{p}^* = \underset{\sim}{f}^* , \tag{18}$$

where ∇ represents an affine connection on the manifold, so that the left hand represents the covariant differential of the generalized momentum $\underset{\sim}{p}^*$ along a path on the manifold with tangent vector $\underline{v}$ [17], so that

$$\nabla_{\underline{v}} \underset{\sim}{p}^* = (\dot{p}_I - \Lambda^L_{JI} p_L v^J) \underset{\sim}{e}^I ,$$

with components of the generalized momentum given by

$$p_I = g_{IJ} v^J . \tag{19}$$

In addition, $\underset{\sim}{f}^*$ represents the generalized applied forces. On manifold X, this law appears in the form

$${}^b\nabla_{\underline{\bar{v}}} \underset{\sim}{\bar{p}}^* = \underset{\sim}{\bar{f}}^* , \tag{20}$$

since the appropriate quantities live in the b-tangent space ${}^bT_p X$ and the b-cotangent space ${}^bT^*_p X$, respectively.

According to the material presented in the previous section, both the metric components and the affinities involved in Newton's law are affected in a significant manner by the presence of the boundary. However, this occurs only within a layer starting at the boundary ∂X of X, with a relatively small width b, introduced by the unilateral constraint examined. On the other hand, it is clear that the laws of motion expressed by Eqs (18) and (20) are identical within the interior X^o of manifold X. This picture is illustrated by Fig. 1. First, in Fig. 1a is depicted the original configuration manifold M, including the constrained configuration manifold X, which results by imposing condition (1). Then, in Fig. 1b is shown a magnified picture of the boundary layer area surrounding the neighborhood of a point p on ∂X. Apart from the special x-coordinate system, originating at p and having axis x^1 normal to the boundary, two curves (γ_α and γ_β) belonging to the special b-vector field $V_b(X)$, passing tangentially through point p with a different curvature, are also shown.

The focus of the present study is now shifted to the interior of the boundary layer. As a first step, this necessitates an appropriate scaling of the terms involved in the equations of motion [18]. This task is most conveniently performed in a local x-coordinate system. Then, using the above analysis and keeping only the dominant terms, it can be shown that for points near the boundary Eq. (20) is replaced by

$$\dot{\hat{p}}_1 - \overline{\Lambda}^1_{11}\hat{p}_1 v^1 - \hat{f}_1 = 0\,. \tag{21}$$

and

$$\dot{p}_i - \Lambda^{\ell}_{ji}\, p_\ell v^j - \overline{f}_i = 0\,, \tag{22}$$

for $i = 2,\ldots,n$. For a frictionless contact, all terms in the last equation are $O(1)$, while those in Eq. (21) are $O(1/x^1)$. For this reason, the repulsive forcing arising within the boundary layer is chosen by the expression

$$\hat{f}_1(x^1,\dot{x}^1) = [\frac{k_1}{x^1} - \frac{c_1\dot{x}^1}{(x^1)^2}]\hat{s}(x^1;a,b)\,. \tag{23}$$

The first term in the right side models the effect of a force generated by a gravity type potential. It represents a strong force pushing the figurative point away from the boundary. On the other hand, the second term is associated with the dissipation of energy taking place during the motion within the boundary layer. Since this force must vanish in the outer region, a smooth function $\hat{s}(x^1;a,b)$ is also included in Eq. (23) in order to guarantee a smooth transition of the boundary force from the inner to the outer region of the boundary layer [12].

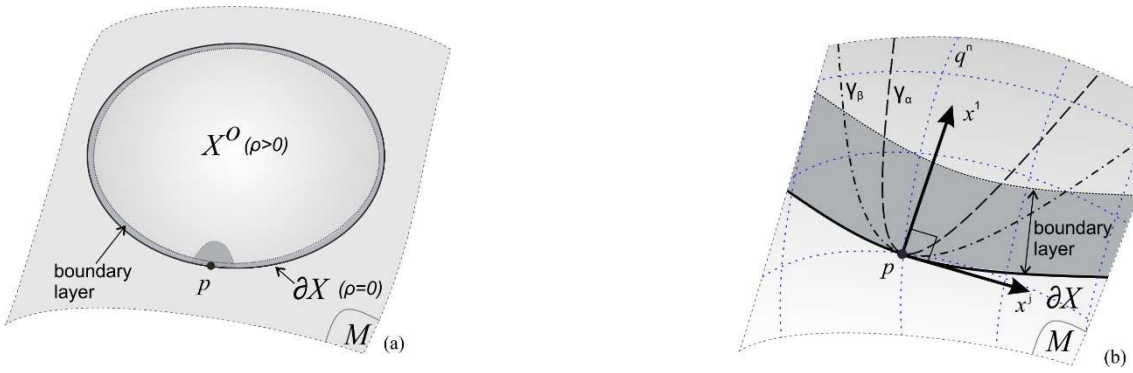

Fig. 1: (a) Original configuration manifold M and constrained manifold X, for a system subject to a unilateral constraint. (b) Magnification around a boundary point p.

The generality of the geometric approach employed makes possible the consideration of contact events arising from the interaction between any combination of particles, rigid bodies and deformable bodies. In accordance to the general setting of Analytical Mechanics, the behavior of these bodies in the physical space, denoted by E^3, is analyzed in the configuration space X of the mechanical system examined. Apart from determining the corresponding geometric properties, this requires a set up of mappings between the physical space and the configuration space. For instance, starting from the kinematics, the relative velocity $\underline{V}$ at the contact point of the two bodies that come in touch in the physical space is related to the generalized velocities through a general linear mapping

$$\underline{V} = D\,\underline{\dot{q}}\,. \tag{24}$$

The column vectors $\underline{V} = V^\alpha \underline{n}_\alpha$ and $\underline{\dot{q}} = \dot{q}^{I'}\underline{e}_{I'}$, with $\alpha = 1,2,3$ and $I' = 1,\ldots,n$, are expressed with respect to the bases $\{\underline{n}_1 \;\; \underline{n}_2 \;\; \underline{n}_3\}$ and $\{\underline{e}_{1'} \;\; \ldots \;\; \underline{e}_{n'}\}$ in the tangent space of the physical and the configuration manifold, respectively. This implies that the dual mapping between the corresponding momenta (covectors) is expressed by

$$\underset{\sim}{p}^* = \underset{\sim}{P}\,D\,, \tag{25}$$

where $\underset{\sim}{p}^*$ and $\underset{\sim}{P}$ are row vectors in the cotangent space of the configuration manifold and the physical space.

If $\tilde{\chi}^\alpha = \chi^\alpha(q^{I'})$ are the coordinates of a point in the physical space with respect to that special coordinate system, the differential of the boundary defining function in the configuration space can be evaluated from

$$d\rho = \frac{\partial \rho}{\partial \underset{\sim}{q}} = \frac{\partial \hat{\rho}}{\partial \underset{\sim}{\chi}} D \quad \Rightarrow \quad d\rho = d\hat{\rho}\, D, \tag{26}$$

with $\hat{\rho} = \rho(\chi(q))$ and $D = \partial \underset{\sim}{\chi} / \partial \underset{\sim}{q}$. Consequently, if $\{\underset{\sim}{n}^1 \quad \underset{\sim}{n}^2 \quad \underset{\sim}{n}^3\}$ is a special basis of the cotangent physical space, selected so that the representative of the base covector $\underset{\sim}{n}^1$, as defined by Eq. (2), is normal to the local plane of contact, Eq. (26) in conjunction with Eq. (25), yields

$$\underset{\sim}{e}^1 = \underset{\sim}{n}^1 D. \tag{27}$$

Based on this, a new basis $\mathfrak{B}^*_{e''} = \{\underset{\sim}{e}^{1''} \quad \dots \quad \underset{\sim}{e}^{n''}\}$ is constructed in the cotangent space ${}^bT^*_pX$, defined by

$$\underset{\sim}{e}^{I''} = A^{I''}_{I'} \underset{\sim}{e}^{I'} = \begin{cases} \underset{\sim}{n}^{I''} D, & I'' = 1,2,3 \\ \delta^{I''}_{I'} \underset{\sim}{e}^{I'}, & I'' = 4,\dots,n \end{cases} \tag{28}$$

Consequently, in order to create a basis for the x-coordinate system, a partial Gram-Schmidt orthogonalization scheme is applied in the form

$$\underset{\sim}{e}^I = \underset{\sim}{e}^{I''} - \gamma^{I''}_J \underset{\sim}{e}^J \quad for \quad I = I'' = 1,...,n \quad and \quad J = 1,2,3, \tag{29}$$

with

$$\langle \underset{\sim}{e}^I, \underset{\sim}{e}^J \rangle = 0 \quad for \quad I \; or \; J = 1,2,3 \; and \quad I \neq J.$$

In this way, combination of Eqs (28) and (29) yields the first three basis vectors in the form

$$\underset{\sim}{e}^J = \underset{\sim}{\eta}^J D \quad for \quad J = 1,2,3,$$

with

$$\underset{\sim}{\eta}^1 = \underset{\sim}{n}^1, \quad \underset{\sim}{\eta}^2 = \underset{\sim}{n}^2 - \gamma^{2''}_1 \underset{\sim}{n}^1 \qquad \underset{\sim}{\eta}^3 = \underset{\sim}{n}^3 - \gamma^{3''}_2 \underset{\sim}{n}^2 + (\gamma^{3''}_2 \gamma^{2''}_1 - \gamma^{3''}_1) \underset{\sim}{n}^1.$$

Next, the components of the generalized force in the configuration space is evaluated in the form

$$\hat{f}_1 = F_1 + \gamma^{2''}_1 F_2 + \gamma^{3''}_1 F_3, \quad \hat{f}_2 = F_2 + \gamma^{3''}_2 F_3 \quad and \quad \hat{f}_3 = F_3. \tag{30}$$

The relation between the normal component F_1 and the two tangential components F_2 and F_3 of the contact force $\underset{\sim}{F}$ is established through an appropriate constitutive law, describing the friction action. For instance, the Amontons-Coulomb law is the most frequently adopted law for calculations in the physical space [2-6]. Moreover, assuming isotropic friction for convenience, it turns out that the admissible domain for the force covector is described by a cone C in the physical space, defined by the relation

$$\| F_2 \underset{\sim}{n}^2 + F_3 \underset{\sim}{n}^3 \|_2 = \sqrt{F_2^2 + F_3^2} \leq \mu \, | F_1 |,$$

where μ is a constant, known as the friction coefficient of the bodies in contact. In particular, the strict inequality holds in case of sticking at the point of contact, while the equality represents a sliding condition. Then, due to the linearity of the mapping expressed by Eq. (25), it can be shown that the friction cone C is transformed into another cone K within the corresponding three dimensional subspace of the cotangent space in the configuration space, with origin at point p. Also, the image of a basis of cone C, which is normal to the axis $\underset{\sim}{n}^1$, remains plane in the configuration space and parallel to the plane defined by the axes $\underset{\sim}{e}^{2''}$ and $\underset{\sim}{e}^{3''}$, as shown in Fig. 2. However, it is not perpendicular to the axis $\underset{\sim}{e}^{1''}$, which is normal to the boundary in the configuration space. Also, a cross-section of C normal to $\underset{\sim}{n}^1$ is circular but becomes elliptic in the configuration space. It remains circular and parallel to the boundary in the configuration space in special cases only, like in a central collision.

Based on the above, it becomes obvious that the presence of friction causes two important effects in the formulation established so far in the configuration space. First, taking into account Eq. (30), it appears that the forcing terms $\hat{f}_2$ and $\hat{f}_3$ should be comparable to $\hat{f}_1$, which means that they should all be of the same order, $O(1/x^1)$, so that the friction can cause tangible effects. Therefore, since the terms $\Lambda^{\ell}_{ji} p_{\ell} v^j$ and $\dot{g}_{ij} v^j$ of Eq. (22)

remain $O(1)$ even inside the boundary layer, the only possible way to balance the aforementioned forcing terms is to assume that the terms $\dot{p}_2$ and $\dot{p}_3$, representing a momentum change, vary rapidly, i.e., they are $O(1/x^1)$ within the boundary layer. This implies that the first two relations in Eq. (22) separate from the rest (i.e., those with $i = 4,...,n$) and appear in the form

$$\dot{p}_2 - \hat{f}_2 = 0 \quad and \quad \dot{p}_3 - \hat{f}_3 = 0\,, \tag{31}$$

where the forcing terms $\hat{f}_2$ and $\hat{f}_3$ are determined by Eq. (30). Moreover, friction affects the amplitude of the forcing in the normal direction. Specifically, the equation of motion along the normal direction to the manifold boundary is expressed by Eq. (21), again, but now with $\hat{f}_1$ given by Eq. (30), where $F_1(\chi^1, \dot{\chi}^1)$ appears in a form similar to that in Eq. (23), with x^1 and $\dot{x}^1$ replaced by χ^1 and $\dot{\chi}^1$, respectively, while F_2 and F_3 are determined by the friction law employed.

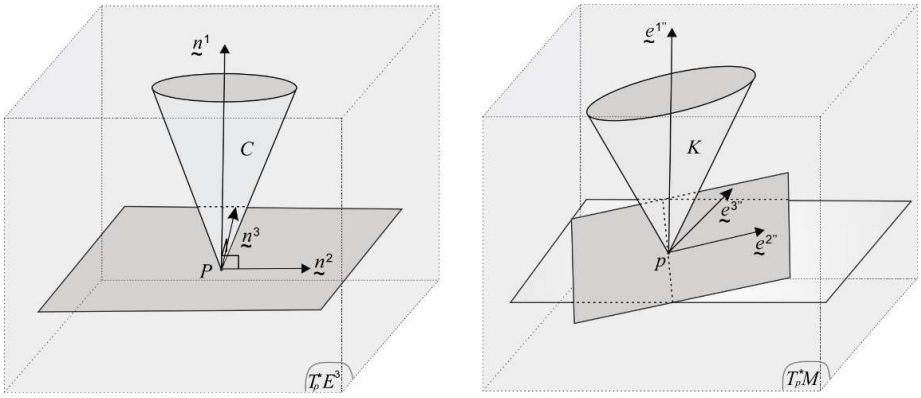

Fig. 2: Friction cone in the physical space and its image in the corresponding three dimensional subspace of the cotangent space in the configuration manifold.

Finally, if a holonomic set of coordinates is employed, represented by the quantity $\underline{q} = (q^1 \quad \cdots \quad q^n)^T$, Eqs (21) and (31) give rise to a set of equations of motion, which can be put in the matrix form

$$M(\underline{q})\,\underline{\ddot{q}} + \underline{h}(\underline{q}, \underline{\dot{q}}, t) = \underline{0}\,, \tag{32}$$

even during the contact phase. This form is coincident with the second order ODE form obtained by classical formulations for systems with no constraints. If non-holonomic coordinates are also involved, then the set of equations of motion is expressed in terms of a set of quasi-velocities in place of $\underline{\dot{q}}$ [15].

5 Comparison with previous formulations

Depending on the treatment of the dynamics during the contact phase, all the previous formulations can be cast in two general categories. In the first and bigger category, methods of non-smooth mechanics are applied (e.g., [2-5]). Specifically, it is assumed that satisfaction of the unilateral constraint requires the generation of a constraint force at the contact point and the equations of motion (32) are put in the form

$$M(\underline{q})\,\underline{\dot{u}} + \underline{h}(\underline{q}, \underline{u}, t) = W(\underline{q})\,\underline{\lambda}\,, \tag{33}$$

where the vectors $\underline{u}$ and $\underline{\dot{u}}$ include the generalized velocities and accelerations, respectively. In addition, the $n \times 3$ matrix $W(\underline{q})$ and the vector $\underline{\lambda}$ appear in the form

$$W(\underline{q}) = [\underline{w}_1 \quad \underline{w}_2 \quad \underline{w}_3] \quad \text{and} \quad \underline{\lambda} = (\lambda_1 \quad \lambda_2 \quad \lambda_3)^T\,,$$

where the vectors $\underline{w}_1$, $\underline{w}_2$ and $\underline{w}_3$ define the normal and the two special tangential directions in the configuration space specified by the mapping with the physical space, while the multipliers λ_1, λ_2 and λ_3 represent the magnitude of the corresponding normal and tangential components of the contact force, respectively. The magnitude of these multipliers is unknown and must be determined by imposing an appropriate impact law [2,3]. For this, the displacements $\underline{q}$ are assumed to be absolutely continuous functions of time, while the velocities $\underline{u}$ are functions of locally bounded variation, with possible discontinuities at the impact times [1]. This permits integration of Eq. (33) over a short contact time interval, where t^- and t^+ is the time instance of the initiation and end of contact, respectively. As a result, the impact equations of the system are put in the form

$$M(\underline{u}^+ - \underline{u}^-) = W\underline{\Lambda} \quad \text{with} \quad \underline{\Lambda} = \lim_{t^+ \to t^-} \int_{t^-}^{t^+} \underline{\lambda}\, dt\,, \tag{34}$$

assuming no detectable change in the position, so that the mass matrix remains constant during the entire contact phase. It is also assumed that the second term in the left hand side of Eq. (33) includes non-impulsive forces and its contribution to Eq. (34) is negligible. Then, taking into account the contact kinematics of the system and combining the last equation with an impact law, like Newton's kinematic or Poisson's kinetic impact law, leads to determination of the post-impact velocity $\underline{u}^+$ and the impulse $\underline{\Lambda}$ [3,4].

The new approach presents some original characteristics when compared to these formulations. First, the new system of equations of motion (21) and (31) constitutes a set of ODEs even during the contact phase. This avoids singular behavior associated with the numerical solution of sets of differential-algebraic equations (DAEs), instead, like Eq. (33) [20]. Also, the whole trajectory is known during the contact phase and there is no need for defining and employing restitution coefficients. However, the most important difference is that the present formulation leads to elimination of the discontinuity in the velocities during the whole contact phase. This is achieved by allowing a rapid increase in the value of the metric and the affinity component along the direction normal to the boundary of the configuration space, which slows down the figurative particle inside the boundary layer in a rapid fashion. At the same time, the forces developed are large but have a bounded magnitude, since the figurative particle never reaches the boundary [12]. In fact, a strong repulsive force is applied on this particle, not related to action of a stiff spring, pushing it away from the boundary.

The elimination of the non-smoothness effects is in accordance to some earlier studies, known as Darboux-Keller approaches [7-10]. These studies investigate also motion of contacting bodies even during the impact phase and lead to an ODE formulation. However, they use the normal impulse as a time-like independent variable, instead. This makes necessary to still employ the idea of a restitution coefficient, in order to predict the end of the contact phase [6]. More importantly, such an approach eliminates the short but finite time scale associated with the contact duration from the equations. The new formulation uses time as the independent variable and, as a consequence, it can handle impact of general bodies, including rigid and deformable bodies, in an effective way. Namely, the duration of the contact phase provides a strong and safe basis for selecting the mode shapes of a structure which have a significant participation in the impact dynamics. Finally, the whole spirit of the new approach is based on different principles than those of the Darboux-Keller approaches, as explained at the end of the previous paragraph.

In closing, it is worth noting that a combination of Eqs (24) and (25) with Eq. (19) yields

$$\underline{V} = \bar{E}\underset{\sim}{P}^T\,, \tag{35}$$

with

$$\bar{E} \equiv D\bar{G}_q^{-1}D^T\,. \tag{36}$$

Moreover, using Eqs (8) and (9) one can write

$$\bar{G} = G + \hat{G}\,,$$

where all the elements of matrix $\hat{G}$ are zero, except for the single element $\hat{g}_{11}$, which is given by Eq. (10). Then, based on Eq. (11), it is straightforward to show that

$$\overline{G}_q = A^T \overline{G} A = G_q + \hat{G}_q ,$$

with transformation matrix $A = [A^I_{I'}]$ and

$$\hat{G}_q = (\underset{\sim}{A}^1)^T \underset{\sim}{A}^1 \hat{g}_{11} , \tag{37}$$

with covector $\underset{\sim}{A}^1 = [A^1_{I'}]$. In this respect, matrix $\overline{G}_q$ is a rank-one correction of G_q. Therefore, application of the Sherman-Morrison formula yields its inverse directly in the form

$$\overline{G}_q^{-1} = G_q^{-1} - \frac{1}{1+\underset{\sim}{A}^1 G_q^{-1} (\underset{\sim}{A}^1)^T \hat{g}_{11}} G_q^{-1} \hat{G}_q G_q^{-1} \equiv G_q^{-1} + \Delta G_q^{-1} .$$

Also, by employing the last result, it is easy to show that

$$\overline{E} = E + D(\Delta G_q^{-1}) D^T = E + \hat{E} , \tag{38}$$

with

$$\overline{E} = \overline{E}^T , \quad E = E^T \quad \text{and} \quad \hat{E} \equiv D(\Delta G_q^{-1}) D^T = \hat{E}^T .$$

Replacing $\overline{E}$ by E in Eq. (35), furnishes an expression given in previous work [6,9], involving components of the differential relative velocity and impulse at the contact point, instead.

6 Examples

In the first example, dynamics of a single particle colliding with a rigid wall is examined, while the second example refers to impact between a rigid body and a half-space. Finally, deformability effects are considered in the last example.

6.1 Collision of a particle with a rigid wall

A single particle with mass m hits a rigid wall. During free motion, its position is determined by three Cartesian coordinates χ^1, χ^2 and χ^3 in the physical space E^3. If the q-coordinates are identical to them, the original configuration space is $M = \mathbb{R}^3$. Then, if these coordinates are selected so that the wall is at $\chi^1 = 0$,

$$\rho(q) = q^1 .$$

Based on Eq. (26), this implies that $D = I_3$, where I_3 is the 3×3 identity matrix, while Eq. (13) yields

$$\underset{\sim}{A}^1 = (1 \quad 0 \quad 0) = \underset{\sim}{n}^1 .$$

Also, the x-coordinate system can be chosen to coincide with the q-coordinate system. Therefore,

$$G = [g_{IJ}] = m I_3 \quad \textit{and} \quad \Lambda^K_{IJ} = 0, \quad (I, J, K = 1, 2, 3).$$

Consequently,

$$G_q^{-1} = G^{-1} = m^{-1} I_3 , \tag{39}$$

so that the metric matrices near the boundary are obtained in the following diagonal form

$$\overline{G} = \overline{G}_q = diag\left(m + m(b/x^1)^2 \quad m \quad m \right)$$

Next, application of Eq. (29) leads to

$$\gamma_1^{2''} = \gamma_1^{3''} = \gamma_2^{3''} = 0 \tag{40}$$

and

$$\underset{\sim}{\eta}^1 = \underset{\sim}{n}^1, \quad \underset{\sim}{\eta}^2 = \underset{\sim}{n}^2 \quad and \quad \underset{\sim}{\eta}^3 = \underset{\sim}{n}^3.$$

Finally, the components of the velocity in the physical space and the force in the configuration space are obtained in the form

$$V^\alpha = \delta_I^\alpha \dot{x}^I = \dot{x}^\alpha \quad and \quad \hat{f}_\alpha = F_\alpha \quad (\alpha = 1,2,3), \tag{41}$$

respectively.

The above information is sufficient to determine the action during the contact phase. First, the governing Eq. (21), is put in the form

$$\frac{d}{dt}\left[\frac{m}{(x^1)^2}v^1\right] + \frac{m}{(x^1)^3}(v^1)^2 - \frac{k}{x^1} + \frac{cv^1}{v^-(x^1)^2} = 0, \tag{42}$$

with

$$k_1 = kb^2 \quad and \quad c_1 = cb^2/v^-.$$

Next, Eqs (31) are put in the form

$$m\dot{v}^2 - \hat{f}_2 = 0 \quad and \quad m\dot{v}^3 - \hat{f}_3 = 0. \tag{43}$$

At this stage, Eq. (42) represents a nonlinear second order ODE in the coordinate x^1 of the particle, which is decoupled from Eq. (43). In fact, for a given set of initial conditions

$$x^1(0) = b \quad \text{and} \quad v^1(0) = -v^-,$$

an analytical solution of Eq. (42) has been found [12] and expressed in the form

$$x^1(t) = be^{\beta(t)} \; v^1(t) = v^-[(e^{-ct/(v^- g_{11})} - 1)\,ak/c - 1]\,e^{\beta(t) - ct/(v^- g_{11})}, \tag{44}$$

with

$$\beta(t) = (v^-)^2[(k + c/a)g_{11}(e^{-ct/(v^- g_{11})} - 1) + ckt/v^-]/c^2.$$

Likewise, Eq. (43) represents two first order ODEs in the velocity components v^2 and v^3. At every time instance, the forcing terms $\hat{f}_2$ and $\hat{f}_3$ are first determined in terms of $\hat{f}_1$, through application of the friction law. Using the initial conditions

$$v^2(0) = v_{T2} \quad \text{and} \quad v^3(0) = v_{T3},$$

this leads eventually to determination of $v^2(t)$ and $v^3(t)$ during the whole contact phase

Next, a selected set of numerical results is presented. First, in Fig. 3a is shown the history of the normal force $\hat{f}_1$ exerted from the boundary to the particle. The results illustrate the effect of the boundary force parameter k, for $c = 0$. The time is normalized by the total duration of the contact phase, t_f. The results of Fig. 3a indicate that the distribution of the normal force $\hat{f}_1$ is symmetric with respect to the line $t = t_f/2$. Also, this force reaches a plateau around the middle of the contact phase for relatively small values of k. This symmetry is broken by the presence of the boundary force dissipation parameter c, as shown in Fig. 3b, for $k = 10$. In fact, a gradual increase in the value of this parameter causes a reduction in the time interval where this force is impulsive.

Likewise, to demonstrate the effects of the friction coefficient μ, in Fig. 4 is presented the history of the tangential velocity of the particle for several values of μ and $c = 0$. Specifically, the results in Figs 4a and 4b were obtained for $k = 1$ and $k = 10$, respectively. In both cases, sufficiently small values of μ lead to conditions

of gross slip, while larger values lead to slip-stick. Moreover, an increase in k favors the development of gross slip. A similar effect is also caused by increasing the magnitude of the dissipation parameter c.

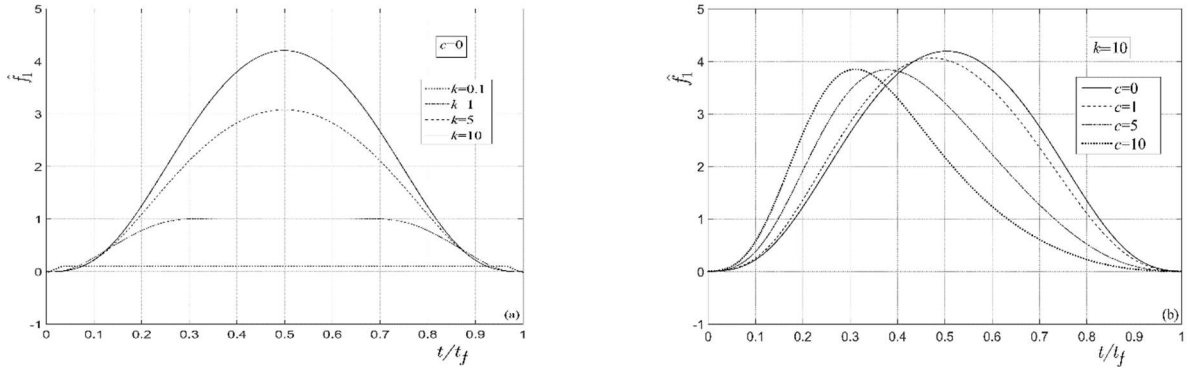

Fig. 3: History of the boundary generated normal force $\hat{f}_1$ on the particle: (a) effect of parameter k, for $c = 0$; (b) effect of parameter c, for $k = 10$.

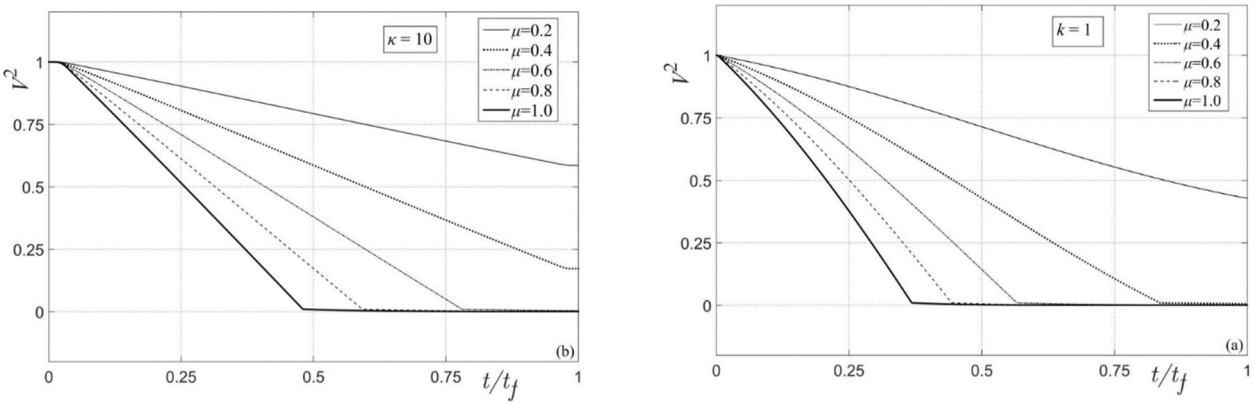

Fig. 4: History of the tangential velocity of the particle for several values of the friction coefficient μ and $c = 0$: (a) $k = 1$ and (b) $k = 10$.

6.2 Collision of a solid body with a rigid wall

In the second example, dynamics of a rigid body colliding with a plane rigid wall in the presence of friction is studied, as shown in Fig. 5. In general, the configuration space of a free rigid body is represented by a six dimensional product space $M \equiv \mathbb{R}^3 \times M(3)$ [19]. The position of the body with respect to an inertial Cartesian reference frame $\mathbb{F}$ in the physical space E^3 is represented by a point on manifold M with generalized coordinates $\underline{q}(t)$ split in two parts, $\underline{q}_C$ and $\underline{q}_R$. The former specifies the position of the center of mass C of the body, while the latter describes the orientation of the body in the physical space. Consequently, the velocity vector is also split in the form $\underline{v}(t) = (\underline{v}_C^T \quad \underline{v}_R^T)^T$, where $\underline{v}_C = \dot{\underline{q}}_C(t)$ and the rotational part is expressed in terms of quasi-coordinates $\underline{\vartheta}$, with

$$\underline{v}_R = \dot{\underline{\vartheta}} \equiv (\Omega^1 \quad \Omega^2 \quad \Omega^3)^T \quad and \quad \dot{\underline{\vartheta}} = T(\underline{q}_R)\dot{\underline{q}}_R,$$

where $T(\underline{q}_R)$ is the tangent operator at $\underline{q}_R$ [20]. Then, based on the kinetic energy of the body, the metric on space M can be selected in the following block diagonal form

$$G_q = [g_{I'J'}] = \begin{bmatrix} mI_3 & 0 \\ 0 & J_C \end{bmatrix}, \tag{45}$$

where m is the mass and J_C is the mass moment of inertia matrix of the body with respect to an orthonormal frame fixed in the body, with origin at its center of mass C. Moreover, the only non-zero affinities $\Lambda^{K'}_{I'J'}$ are

$$\Lambda^{4'}_{5'6'} = -\Lambda^{4'}_{6'5'} = \Lambda^{5'}_{6'4'} = -\Lambda^{5'}_{4'6'} = \Lambda^{6'}_{3'5'} = -\Lambda^{6'}_{5'3'} = 1. \tag{46}$$

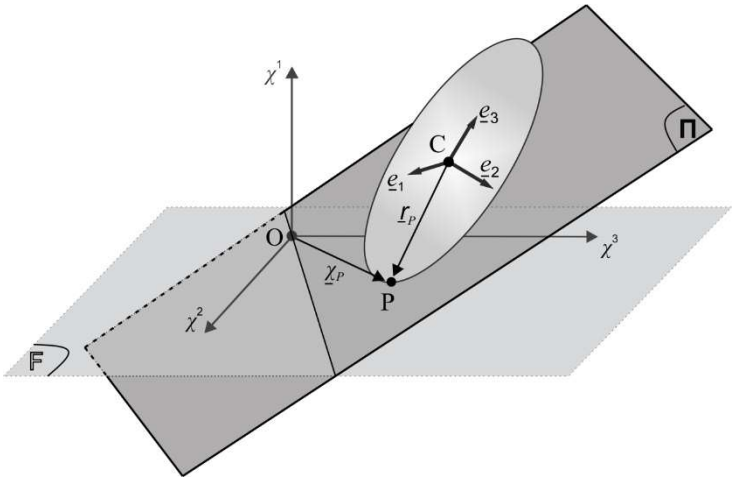

Fig. 5: A rigid body hitting a rough half-space.

Next, consider a point P of the body, which at some instance comes in contact with a plane rigid wall Π. In the physical space, this wall is defined by the function

$$s(\underline{\chi}) = \sum\nolimits_{\alpha=1}^{3} s_\alpha \chi^\alpha = 0, \tag{47}$$

where $\underline{\chi} = (\chi^1 \quad \chi^2 \quad \chi^3)^T$ is the position vector of a point on this plane with respect to $\mathbb{F}$. This can be considered as the boundary defining function in the physical space. In addition, the position vector of the contact point P with respect to frame $\mathbb{F}$ is given by

$$\underline{\chi}_P = \underline{\chi}_C + R(\underline{q}_R)\,\underline{r}_P, \tag{48}$$

where $\underline{\chi}_C = \underline{q}_C$ and R is a 3×3 rotation matrix, fixing the orientation of the body with respect to $\mathbb{F}$, while $\underline{r}_P$ is the position vector of point P with respect to the body frame [20]. Then, direct differentiation of Eq. (48) leads to

$$\underline{V}_P = \underline{v}_C + \dot{R}\,\underline{r}_P,$$

with $\dot{R} = R\tilde{\Omega}$ and eventually, after a trivial manipulation, to Eq. (24) with transformation matrix

$$D = [I_3 \quad -R\tilde{r}_P]. \tag{49}$$

The entities $\tilde{\Omega}$ and $\tilde{r}_P$ represent 3×3 skew-symmetric matrices having $\underline{\Omega}$ and $\underline{r}_P$ as axial vectors, respectively [19,20]. Moreover, the unilateral constraint for the contact event examined is expressed by

$$\rho(\underline{q}) \equiv s(\underline{\chi}_P) \geq 0, \tag{50}$$

which yields the boundary defining function in the configuration space. Using the last expression, one can also arrive at Eq. (49) in an alternative way, through application of Eq. (26). Specifically, based on their definition by Eq. (13), the elements of the special covector

$$\underset{\sim}{A}^1 \equiv [A^1_{I'}] = \frac{\partial \rho}{\partial \underline{q}} = \left(\frac{\partial \rho}{\partial \underline{q}_C} \quad \frac{\partial \rho}{\partial \underline{\vartheta}}\right),$$

can be evaluated and put in the form

$$\underset{\sim}{A}^1 = \underset{\sim}{s}\, D \text{, with} \quad \underset{\sim}{s} = (s_1 \quad s_2 \quad s_3) \tag{51}$$

and matrix D given by Eq. (49). In addition, using Eq. (45) leads eventually to

$$E = m^{-1} I_3 - R\,\tilde{r}_P\, J_C^{-1}\, \tilde{r}_P\, R^T , \tag{52}$$

with matrix $E = [e_{\alpha\beta}]$. Then, application of Eq. (29), together with Eqs (27) and (28) yields

$$\gamma_1^{2''} = \frac{\langle \underset{\sim}{e}^{2''}, \underset{\sim}{e}^1 \rangle}{\langle \underset{\sim}{e}^1, \underset{\sim}{e}^1 \rangle} = \frac{(\underset{\sim}{n}^2 D) G_q^{-1} (\underset{\sim}{n}^1 D)^T}{(\underset{\sim}{n}^1 D) G_q^{-1} (\underset{\sim}{n}^1 D)^T} = \frac{\underset{\sim}{n}^2 E (\underset{\sim}{n}^1)^T}{\underset{\sim}{n}^1 E (\underset{\sim}{n}^1)^T} = \frac{e_{21}}{e_{11}}$$

and

$$\gamma_1^{3''} = \frac{e_{31}}{e_{11}} \quad \textit{and} \quad \gamma_2^{3''} = \frac{\underset{\sim}{n}^3 E (\underset{\sim}{n}^2)^T}{\underset{\sim}{\eta}^2 E (\underset{\sim}{\eta}^2)^T} = \frac{e_{32}}{e_{22} - \gamma_1^{2''}(e_{21} + e_{12}) + (\gamma_1^{2''})^2 e_{11}} .$$

6.2.1 Collision of a rigid spheroid with a half-space

First, consider a homogeneous rigid spheroid (i.e., an ellipsoid of revolution), with mass m and radii r, r and r', aligned with the axes of a Cartesian coordinate system in the physical space when hitting a rigid wall, as shown in Fig. 6a. The contact point P lies on the intersection of its circular equator with the χ^1-axis.

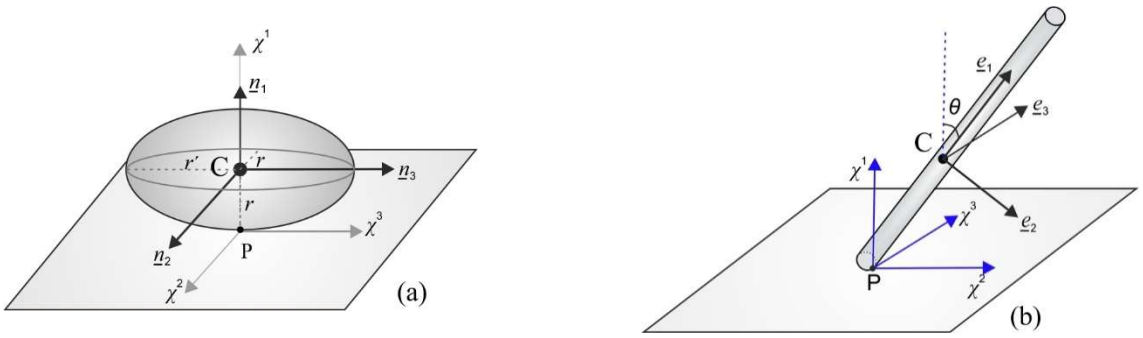

Fig. 6: (a) A spheroid and (b) a bar, hitting a rough half-space.

The set of results presented in Fig. 7a are hodographs obtained for $k = 10$, $c = 0$ and three values of the ratio J_{11}/J_{33}, corresponding to an oblate spheroid, a sphere and a prolate spheroid. In all cases, the spheroid hits the ground with an initial normal velocity $V^1(0) = -1$ and zero angular velocity with respect to the wall. Also, the initial components of the velocities in the plane of the wall are $V^2(0) = 1$ and $V^3(0) = 1$, as indicated by the coordinates of point A. For relatively small values of μ, the spheroid undergoes gross slip. For instance, points B, C and D on the three hodographs examined indicate the end of the contact phase for μ=0.1. Also, the hodographs selected end up at point (0,0) for the limiting values μ=0.18, 0.20 and 0.28, corresponding to J_{11}/J_{33} =8/5, 1 and 2/5, respectively. Then, a final stick state is reached for larger values of μ. Clearly, the sliding direction varies during the motion for the case of the oblate or prolate spheroid. In the case of a sphere, where J_{11}/J_{33} =1, the hodograph is an isocline [8,9].

Finally, in Fig. 7b are presented the histories of the two tangential components of the velocity of the contact point for J_{11}/J_{33} =2/5 and two characteristic values of μ. First, results are shown for μ=0.16, which is smaller than the critical value leading to final stick. Clearly, this leads to conditions of gross slip. Similar results are also presented for μ=0.20, which is a bit larger than the critical value. The results verify that the contact event finishes now with a stick phase.

The case examined corresponds to a central collision. Then, like for the case of a particle, Eq. (30) leads to Eq. (41), which shows that the force in the normal direction is not affected by the forces in the tangential directions, leading to conditions of a balanced collision [8]. This implies that the dynamics of the central collision of a rigid sphere with a half-space is in essence identical to the dynamics during collision of a particle with a plane, which was investigated in subsection 6.1. For this reason, only a comparison between numerical and experimental results is performed next, obtained by using data reported in an earlier work [21]. Specifically, in Fig. 8 are compared results referring to the normal component of the force for two selected values of the initial incidence angle, defined by

$$\varphi = \tan^{-1}[-V^3(0)/V^1(0)] .$$

The numerical and experimental results presented for both the smaller value $\varphi = 20^o$ (Fig. 8a) and the larger value $\varphi = 60^o$ (Fig. bb) are in close agreement.

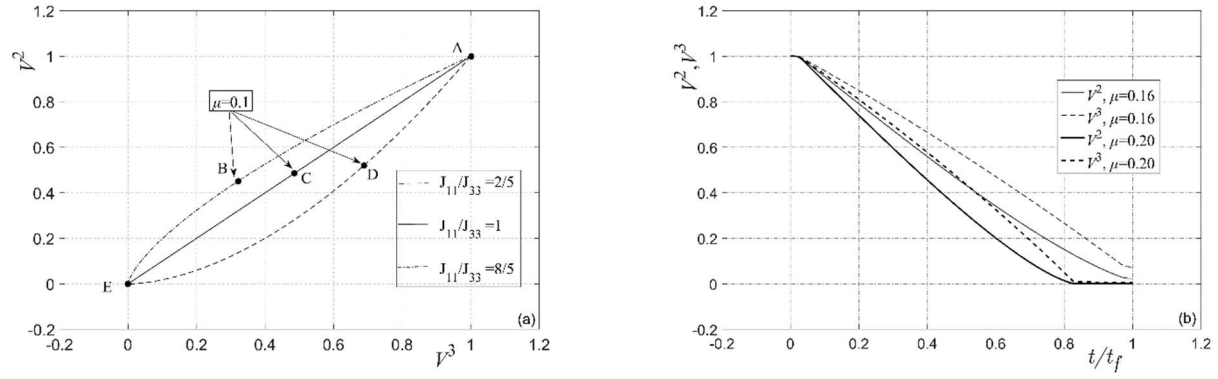

Fig. 7: Collision of a spheroid with a plane: (a) hodographs starting at (V^2 , V^3)=(1,1); (b) tangential velocity components of the contact point for J_{11}/J_{33} =2/5 and μ =0.16 or 0.20.

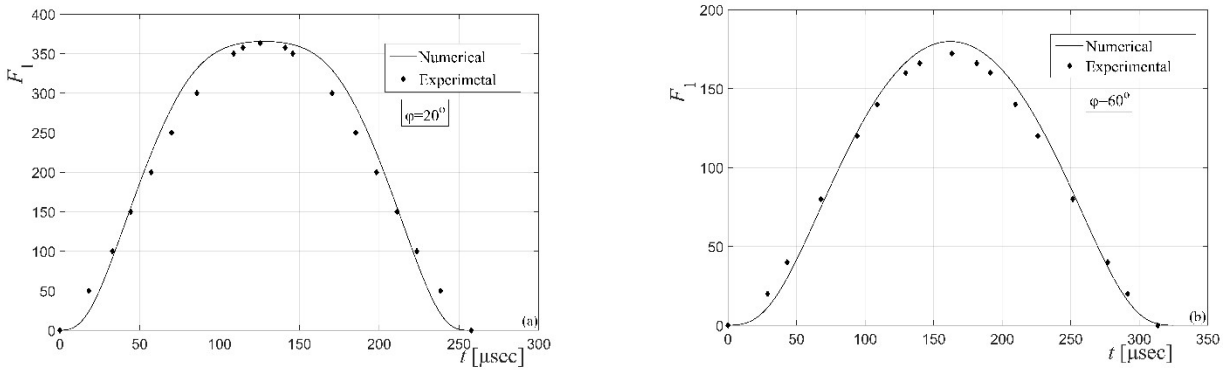

Fig. 8: Comparison of numerical and experimental results for central oblique impact of a sphere. Normal force for: (a) $\varphi = 20^o$ and (b) $\varphi = 60^o$.

6.2.2 Oblique collision of a rigid rod with a half-space

The last set of results refers to collision of a homogeneous rigid cylinder with mass m , length 2ℓ and radius r with a rough half-space, as shown in Fig. 6b. The longitudinal axis of the cylinder lies in the plane $O\chi^1\chi^2$ and makes an angle θ with the axis $O\chi^1$. First, in Fig. 9a are presented hodographs, originating from the same point

of the plane (V^2, V^3), for $k=10$, $c=0$ and several values of μ. The value of angle θ is selected to be equal to 1.10 rad, so that two critical friction parameter values are determined as $\bar{\mu}$=0.7499 and μ_*=0.5721 [6,9]. For $\mu < \mu_*$, conditions of gross slip are observed, while the shape of the hodographs demonstrate that the sliding direction varies continuously during the motion. At the critical value $\mu = \mu_*$, the hodograph becomes an almost straight line (isocline). In addition, following a temporary stick, the sliding direction changes but remains constant and parallel to the χ^2-axis throughout the subsequent motion. For $\mu < \mu_* < \bar{\mu}$, the tangential velocity becomes zero at some instance but continuous slipping immediately afterwards. Finally, for $\mu > \bar{\mu}$, once the stick state appears it persists until the end of the contact phase. Finally, in Fig. 9b are presented hodographs obtained for three different values of parameter k. The results verify that as the value of k is increased gradually, leads to the appearance of an isocline on plane (V^2, V^3).

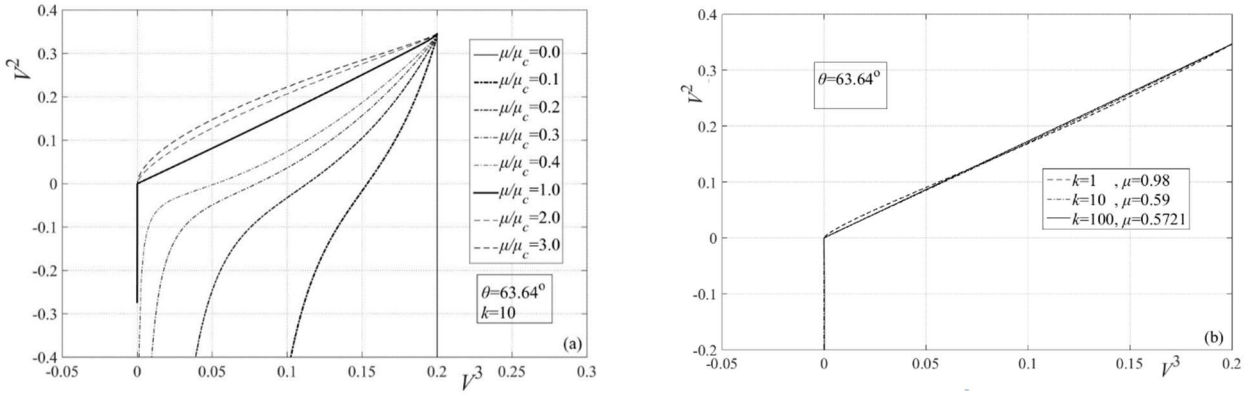

Fig. 9: Hodographs for collision of a bar with a rough half-space, for different values of: (a) μ and (b) k.

6.2.3 Collision between rigid and flexible bodies

In closing, it is mentioned that the analysis developed is applicable to the most general single point collision, involving any combination of mechanical bodies. The most essential information needed for this includes the geometric properties of the configuration manifold and the transformation matrix D. For instance, when two rigid bodies collide, the dimension of the configuration manifold increases to 12. Moreover, the corresponding metric components and the affinities are selected in a way similar to that followed in Section 6.2. In addition, consideration of the corresponding kinematics leads easily to

$$D = [I_3 \quad -R\tilde{u}_P \quad -I_3 \quad R'\tilde{u}'_P],$$

where the quantities R' and $\tilde{u}'_P$ are associated with the second body.

Likewise, the same analysis can also be applied to configurations involving deformable bodies, obeying general constitutive laws. As the simplest example in this category, consider a flexible body hitting a rigid half-space. It is first assumed that the body has already been discretized geometrically, based on some appropriate dynamic considerations, so that its flexibility effects are described in a sufficiently accurate manner by n elastic modes. Then, the configuration manifold of the free body is represented by an $(n+6)$-dimensional product space $M \equiv \mathbb{R}^3 \times M(3) \times \mathbb{R}^n$ [11,19]. This means that the generalized coordinates $\underline{q}(t)$ are now split in three parts, $\underline{q}_C$, $\underline{q}_R$ and $\underline{q}_F$, so that the position vector of the contact point P with respect to frame $\mathbb{F}$ (see Fig. 6) is given by

$$\underline{\chi}_P = \underline{q}_C + R(\underline{q}_R)(\underline{r}_P + \Phi \underline{q}_F),$$

where Φ is a $3 \times n$ matrix, furnishing the flexible part of the displacement [20]. Then, direct differentiation of the last equation leads to Eq. (24), with

$$D = [I_3 \quad -R\tilde{u}_P \quad R\Phi],$$

while

$$\underline{u}_P = \underline{r}_P + \Phi \underline{q}_F \quad \text{and} \quad \underline{v}(t) = (\dot{\underline{q}}_C^T \quad \underline{\Omega}^T \quad \dot{\underline{q}}_F^T)^T .$$

Again, the unilateral constraint for the contact event examined is expressed by Eq. (50). Finally, the metric G_q on space M can be selected by considering the total kinetic energy of the body, while the corresponding affinities are also determined easily, based on the product form of the configuration manifold.

7 Synopsis and extensions

In the first part of this study, an analysis was presented on the dynamics of general single point frictional collision between two mechanical bodies. This analysis was performed within the framework of analytical dynamics, by employing some key concepts of differential geometry. First, a boundary was constructed for the original configuration manifold by using the condition of no impenetrability. Then, the essential geometric properties of the constrained manifold were determined. This provided the foundation for applying Newton's law of motion and led to an elegant geometric picture. Specifically, the motion during the contact phase was found to be governed by a set of three ODEs, when expressed in a special coordinate system in the close vicinity of the configuration boundary, having one axis normal to the boundary and the remaining axes tangent to the boundary. The inertia of the figurative particle representing the motion of the system was found to increase rapidly as it approaches the boundary along this axis. At the same time, a strong repulsive force arises pushing this particle away from the boundary. In addition, friction was found to activate action along two special tangential directions only, determined by a mapping with the physical space. Finally, the equations of motion in the original coordinate system were simply obtained by a proper projection of these three ODEs. In the second part, the study focused on investigating several phenomena arising during frictional contact, by using selected examples.

The new formulation was developed in a systematic way, which provides a firm basis for attacking more challenging problems, like those involving multiple contacts. For this, there already exists a sound theoretical background, based on the theory of manifolds with corners [22,23]. In addition, the enhanced understanding provided by the geometric interpretation of the collision phenomenon studied is expected to lead to development of more accurate and efficient numerical techniques for determining the dynamics of the class of systems examined. This is closely related to development and application of suitable contact detection methods and will also help in developing more effective and robust optimization and control algorithms.

References

[1] J.J. Moreau and P.D. Panagiotopoulos, *Nonsmooth Mechanics and Applications*, CISM Courses and Lectures, vol. 302, Wien: Springer-Verlag, 1988.

[2] F. Pfeiffer and Ch. Glocker, *Multibody Dynamics with Unilateral Contacts*, New York: J. Wiley & Sons, 1996.

[3] Ch. Glocker, *Set-Valued Force Laws*, Dynamics of Non-Smooth Systems, Berlin: Springer, 2001.

[4] R.I. Leine and H. Nijmeijer, *Dynamics and Bifurcations of Non-Smooth Mechanical Systems*, Berlin: Springer-Verlag, 2013.

[5] B. Brogliato, *Nonsmooth Mechanics: Models, Dynamics and Control*, London: Springer-Verlag, 3 ed., 2016.

[6] W.J. Stronge, *Impact Mechanics*, Cambridge UK: Cambridge University Press, 2000.

[7] J.B. Keller, "Impact with friction", *ASME J. Appl. Mech.,* vol. 53, pp. 1–4, 1986.

[8] J.A. Batlle and A.B. Condomines, "Rough collisions in multibody systems," *Mech. Mach. Theory*, vol. 26, pp. 565–577, 1991.

[9] Z. Zhen and C. Liu, "The analysis and simulation for three-dimensional impact with friction," *Multibody Syst. Dyn.,* vol. 18, pp. 511-530, 2007.

[10] W.J. Stronge, "Smooth dynamics of oblique impact with friction," *Int. J. Impact Eng.*, vol. 51, pp. 36–49, 2013.

[11] E. Paraskevopoulos and S. Natsiavas, "On application of Newton's law to mechanical systems with motion constraints," *Nonlinear Dyn.*, vol. 72, pp. 455-475, 2013.

[12] E. Paraskevopoulos and S. Natsiavas, "A geometric solution to the general single contact frictionless problem by combining concepts of analytical dynamics and b-calculus," *Int. J. Non-Linear Mech.*, vol. 95, pp. 117-131, 2017.

[13] R.B. Melrose, *The Atiyah-Patodi-Singer Index Theorem*, Research Notes in Mathematics, vol. 4, Wellesley MA.: A.K. Peters Ltd, 1993.

[14] N.S. Nguyen and B. Brogliato., *Multiple Impacts in Dissipative Granular Chains*, Lecture Notes in Applied and Computational Mechanics, vol. 72, Berlin: Springer, 2014.

[15] J.G. Papastavridis, *Tensor Calculus and Analytical Dynamics*, Boca Raton: CRC Press, 1999.

[16] A.M. Bloch, *Nonholonomic Mechanics and Contro*l, New York: Springer-Verlag New York Inc., 2003.

[17] S. Natsiavas and E. Paraskevopoulos, "A set of ordinary differential equations of motion for constrained mechanical systems," *Nonlinear Dyn.*, vol. 79, pp. 1911-1938, 2015.

[18] J. Kevorkian and J.D. Cole, *Perturbation Methods in Applied Mathematics*, New York: Springer-Verlag, 2nd ed., 1985.

[19] E. Paraskevopoulos and S. Natsiavas, "A new look into the kinematics and dynamics of finite rigid body rotations using Lie group theory," *Int. J. Solids Struct.*, vol. 50, pp. 57-72, 2013.

[20] M. Geradin and A. Cardona, *Flexible Multibody Dynamics: A Finite Element Approach*, New York: John Wiley & Sons, 2001.

[21] P.P. Garland and R.J. Roberts, "Comparison of contact forces during oblique impact," in: G.E. Stavroulakis (Ed.), Recent Advances in Contact Mechanics, LNACM 56, pp. 239-255, Springer-Verlag, Berlin, 2013.

[22] R.B. Melrose, "Calculus of conormal distributions on manifolds with corners," *Int. Math. Res. Not. IMRN*, pp. 51–61, 1992.

[23] D. Joyce, "A generalization of manifolds with corners," *Advances Math.*, vol. 299, pp. 760–862, 2016.